NeuroImage 201 (2019) 116003

Contents lists available at ScienceDirect

NeuroImage

journal homepage: www.elsevier.com/locate/neuroimage

Default mode and visual network activity in an attention task: Direct measurement with intracranial EEG

Jiajia Li [a,e], Sharif I. Kronemer [a,b], Wendy X. Herman [a], Hunki Kwon [a], Jun Hwan Ryu [a], Christopher Micek [a], Ying Wu [e], Jason Gerrard [d], Dennis D. Spencer [d], Hal Blumenfeld [a,b,c,d,*]

[a] Neurology, Yale University, New Haven, CT, USA
[b] Interdepartmental Neuroscience Program, Yale University, New Haven, CT, USA
[c] Neuroscience, Yale University, New Haven, CT, USA
[d] Neurosurgery, Yale University, New Haven, CT, USA
[e] State Key Laboratory for Strength and Vibration of Mechanical Structures, School of Aerospace Engineering, Xi'an Jiaotong University, Xi'an, China

ARTICLE INFO

Keywords:
Electrocorticography
fMRI
Consciousness
Default mode network
Broadband gamma

ABSTRACT

Dynamic attention states are necessary to navigate the ever changing task demands of daily life. Previous investigations commonly utilize a block paradigm to study sustained and transient changes in attention networks. fMRI investigations have shown that sustained attention in visual block design attention tasks corresponds to decreased signal in the default mode and visual processing networks. While task negative networks are anticipated to decrease during active task engagement, it is unexpected that visual networks would also be suppressed during a visual task where event-related fMRI studies have found transient increases to visual stimuli. To resolve these competing results, the current investigations utilized intracranial EEG to directly interrogate visual and default mode network dynamics during a visual continuous performance task. We used the electrophysiological data to model expected fMRI signals and to maximize interpretation of current results with previous investigations. Results show broadband gamma power decreases in the default mode network, corresponding to previous EEG and fMRI findings. Meanwhile, visual processing regions including the primary visual cortex and fusiform gyrus demonstrate both sustained decreases during task engagement and stimuli-driven transient increases in gamma power. Modeled fMRI based on gamma power reproduces signal decreases reported in the fMRI literature, and emphasizes the insensitivity of fMRI to transient, regularly spaced signal changes embedded within sustained network dynamics. The signal processing functions of the dynamic visual and default mode network changes explored in this study are unknown but may be elucidated through further investigation.

1. Introduction

Sustained attention to the external world is required to succeed in the myriad tasks of daily life, for example, engaging in conversation, following a recipe, or playing a game. It is equally important to be able to rapidly disengage from states of internal reflection to externally oriented attention, for example, when switching from passive introspection while driving to actively evading obstacles on a difficult section of the road. The neural mechanisms that underlie sustained and transient attentional states are still under investigation. A powerful convergence of evidence from numerous neuroimaging studies suggests that states of external attention are associated with sustained decreased activity in the default mode network (DMN) (Raichle and Snyder, 2007; Shulman et al., 1997; Singh and Fawcett, 2008). However, functional neuroimaging studies do not always accurately reflect underlying neuronal activity (Mishra et al., 2011; Schridde et al., 2008). Due to the medial position of major DMN cortical structures, it is challenging to measure electrophysiological activity in the human DMN. Therefore, compared to networks in lateral cortical regions (e.g., dorsal attention network) the DMN is relatively less examined despite its importance to the field. Previous intracranial electrophysiological records in humans largely correspond with neuroimaging finding in DMN, including increased activity in DMN for internally-directed tasks (e.g., memory or imagining) and decreased activity for externally-directed tasks (e.g., arithmetic or reading), and the magnitude of suppression is mediated by task characteristics, including complexity and difficulty (Foster et al., 2012; Fox et al., 2018; Jerbi et al.,

* Corresponding author. Yale Depts. Neurology, Neuroscience, Neurosurgery, 333 Cedar Street, New Haven, CT, 06520-8018, USA.
E-mail address: hal.blumenfeld@yale.edu (H. Blumenfeld).

https://doi.org/10.1016/j.neuroimage.2019.07.016
Received 19 December 2018; Received in revised form 23 May 2019; Accepted 6 July 2019
Available online 8 July 2019
1053-8119/

2010; Miller et al., 2009; Ossandon et al., 2011; Ramot et al., 2012). Intracranial electrophysiology also suggests heterogeneity in both the spatial and temporal signal characteristics within DMN depending on task demands (Dastjerdi et al., 2011; Fox et al., 2018; Ossandon et al., 2011).

Outside the default mode, studies of visual attention emphasize regions that are activated during task including so-called task positive networks (Dosenbach et al., 2006; Fox et al., 2005). However, modulation of sustained visual attention may also be related to activity *decreases* in regions outside the DMN, which have been relatively-little investigated especially with direct electrophysiological measurements in the human or non-human primate brain (Lachaux et al., 2008; Ossandon et al., 2011; Ramot et al., 2012; Shmuel et al., 2006).

A common approach to recruit both sustained and transient attentional states is by use of a combined block and event design paradigm, for example, the continuous performance task (CPT) (Riccio et al., 2002). These paradigms have multiple variants, but most involve interleaved task phases that contain a stream of stimuli and are commonly coupled with functional magnetic resonance imaging (fMRI) for whole-brain imaging. A primary advantage of the block design paradigm is that it provides analysis of both block and event-related signal embedded within task phases. The core findings from previous block design fMRI studies include transient blood-oxygen-level-dependent (BOLD) increases in multiple regions followed by sustained *increases* in task-positive network regions, including the anterior insula, frontal operculum, and dorsal midline frontal cortex, along with sustained *decreases* in the DMN, for example, the precuneus/posterior cingulate (PC), posterior inferior parietal lobule (PIPL), ventral medial prefrontal cortex (VMP), and anteromedial temporal cortex (AMT) (Dosenbach et al., 2006; Gonzalez-Castillo et al., 2012; Killory et al., 2011; Liu et al., 2011; Rushworth et al., 2002; Singh and Fawcett, 2008; Sohn et al., 2000). Prior event-related analysis of visual stimuli during tasks has shown transient fMRI increases in primary visual cortex (V1) and visual association cortex regions such as the fusiform gyrus (FG), and these transient increases are magnified by directed attention (Corbetta and Shulman, 2002; Harris et al., 2016; Liu et al., 2011; Singh and Fawcett, 2008; Smith et al., 2000). However, relatively few studies have examined the more puzzling sustained *decreases* in fMRI signal that have been observed in visual cortex during task blocks (Gonzalez-Castillo et al., 2012; Killory et al., 2011; Olsen et al., 2013; Singh and Fawcett, 2008; Smith et al., 2000, 2004). Previous human intracranial electrophysiological studies suggest transient suppression of gamma power in visual cortex and DMN that may correspond with decreases in fMRI signal (Lachaux et al., 2005; Ossandon et al., 2011). Therefore, our goal was to examine both sustained and transient electrophysiological signals in these regions through direct human recordings and relate these electrophysiological signals to neuroimaging findings.

Relating sustained block-level and transient event-level changes to their source neural mechanisms is challenging with fMRI due to the poor temporal resolution of the hemodynamic response function (HRF). Also, while positive BOLD responses are linked to increases in population neuronal firing, decreases in BOLD response, as found in the sustained responses in the DMN during attentional tasks are more challenging to interpret due to multiple possible neuronal and vascular underpinnings, for example, vascular steal (Bressler et al., 2007; Liu et al., 2011; Mullinger et al., 2014; Shmuel et al., 2006). For these reasons, high temporal resolution electrophysiological recordings are ideal to directly compare sustained and transient signal changes and to assess the neuronal source of BOLD signal decreases. Measurement of broadband gamma frequency (40–150 Hz) power with intracranial electroencephalography (EEG) has recently been demonstrated to provide an excellent marker of local population neuronal firing in the cerebral cortex (Miller, 2010; Miller et al., 2014; Mukamel et al., 2005). Previous human intracranial EEG studies of the DMN although important, have been relatively limited, showing sustained gamma power decreases with prolonged task epochs but not in a true block design, and with a relatively small number of electrodes and patients (Miller et al., 2009); or showing transient event-related (i.e., single trial) decreases without investigating sustained changes linked to task blocks that represents state versus stimulus-level effects (Jerbi et al., 2010; Ossandon et al., 2011). Ossandon et al. (2011), while not analyzing gamma power changes associated with task blocks, found longer suppression in gamma power in DMN for more cognitively demanding trails, suggesting a sustained cognitive state-dependent modulation of gamma power in DMN. Finally, these studies do not compare sustained and transient signal dynamics in DMN and visual networks.

The current investigation aims to clarify the sustained and transient network changes associated with dynamic attentional demands in classic task-negative networks (e.g., DMN) as well as in the primary visual and visual association cortex. To extend on previous findings, the current investigation utilizes a combined block and event-level visual task in participants with intractable epilepsy implanted with a larger number of intracranial EEG electrodes, offering extensive bilateral cortical surface coverage. To maximize the interpretation between the current results and previous fMRI studies, EEG broadband gamma frequency range was analyzed for its link to population neuronal firing and the BOLD response (Miller, 2010; Miller et al., 2014; Mukamel et al., 2005) and EEG signal transformations were applied to model BOLD response characteristics. We hypothesize that in correspondence with previous fMRI findings, both the DMN and visual processing networks will exhibit sustained broadband gamma activity decreases while sustained attention is engaged by task phases, whereas visual network regions will exhibit transient event-level signal increases.

2. Materials and Methods

2.1. Participants and subdural electrodes

All human participant procedures were approved by the Yale University Institutional Review Board and completed in accordance with the Declaration of Helsinki. Adult participants with intractable epilepsy (N = 11; females = 6; mean age = 35.5, range 23–54 years old) undergoing intracranial EEG implantation for seizure monitoring at the Yale Epilepsy Surgery Program were recruited to participate in the current investigation after written informed consent. The intracranial electrode number and placement were determined by the clinical team, and included subdural grids, strips, and depth electrodes all with 10 mm spacing between adjacent electrode contact centers. Participants were implanted with between 114 and 286 subdural and depth electrode contacts per subject (mean 201 electrode contacts). Across the 11 participants included in the current investigation, there were a total of 2,206 intracranial electrode contacts implanted. Of these, 298 were excluded from analysis because they were located in white matter determined by visual inspection of co-registered whole-brain computed tomography (CT) and structural MRI. The remaining 1,908 electrodes offered bilateral cortical coverage (Fig. 1B).

2.2. Continuous performance task (CPT)

Participants were asked to complete the CPT task. This paradigm has a number of variants and is commonly utilized to examine mechanisms of attention and perception in both healthy and clinical populations (Bai et al., 2010; Beck et al., 1956; Berman et al., 2010; Killory et al., 2011; Mirsky and Rosvold, 1963; Riccio et al., 2002). The CPT paradigm administered in the current investigation involves interleaved 32-second rest and 32-second active task phases (Fig. 1A). During the rest phase, participants were instructed to passively view a white fixation cross (width and height, visual angle = 1.21°) shown at the center of the screen on top of a black background. During the active phase, participants were instructed to (1) maintain fixation at the center of the screen where a string of random, white, capital English letters (A, B, C, D, E, F, G, H, I, L, M, N, O, T, Y, X, Z) were presented at a rate of 1 Hz and (2) to make a

button press with their right thumb using a response box (In-Line Trainer, Current Designs, Inc., SKU OTR-1x4-L) whenever the target stimulus, the letter X, appeared. Each letter was displayed for 250 ms followed by a 750 ms blank period of only the black screen until the onset of the subsequent letter or onset of the rest phase (Fig. 1A). The screen luminance was constant between the rest and task phases to eliminate the influence of low-level task features defining the modulation of signal between CPT rest and task phases. Each task phase block presented 32 letters (height, visual angle = 1.75°) presented once per second in random order, of which 23.5% were the target letter X. Each fixation phase block also lasted for 32 s. Each behavioral run began with a fixation block and then alternated with task for a total of 5 blocks of fixation and 5 blocks of task or a total of 640s per run. The task was coded in Python with PsychoPy version 1.83 (www.psychopy.org) and presented on a laptop computer equipped with a NVIDIA GeForce graphics card and 15.6-inch screen display.

To ensure participant comfort and safety, testing was completed while the participant remained in their hospital bed. A bedside table was oriented in front of the participant and the testing laptop screen placed 85 cm from the nose of the participant. During testing, all lights were turned off and window blinds drawn to control ambient lighting across participants and testing sessions. Participants completed a range of 42–120 rest-task blocks across multiple testing sessions.

2.3. Intracranial EEG data acquisition and epoch extraction

The EEG data were recorded with Natus Neurolink/Braintronics amplifier and pruned using Natus NeuroWorks software (www.neuro.natus.com) at the Yale New Haven Hospital epilepsy monitoring unit. Electrodes were sampled at 1024 Hz with hardware bandpass filter set between 0.1 Hz and 400 Hz. One participant's electrodes were sampled at 256 Hz and data were interpolated in MATLAB and resampled to correspond to a 1024 Hz sampling rate. The reference electrode was selected on a participant-level basis by the clinical team to reduce visible EEG artifact noise.

CPT event time synchronization with EEG recordings was achieved with a transistor-transistor logic (TTL) pulse delivered at the onset of task events (button presses, letter presentations, and rest/active phase onsets) by the experimental laptop computer to an open recording channel of the EEG recording system. The duration of the TTL pulses differed by event type to allow discrimination among events. Block and event-level epochs were extracted for further analysis. Block epochs were 66s in duration, centered to the CPT task phase, including 16s of the rest phase prior to and following the corresponding task phase, and 1s additional "padding" on each end prior to digital filtering. The event epochs were 4s in duration, with 2s of data centered at the onset of each letter stimulus and again with 1s of padding on each end. The first three letters of each block were excluded in the event epoch extractions (but not the block epochs) because we observed a transient increase in signal corresponding to task onset that differentiated these initial event epochs from the remaining letter epochs. The first three letters were included in the block epoch analyses to allow continuity of the timecourse display for blocks (Fig. 2B), however, removing the first three letters had no effect on the block statistical analysis (data not shown).

2.4. Intracranial EEG artifact rejection

All data containing clinical or subclinical epileptic events were rejected from analysis. Remaining extracted block or event-level epochs were passed through an in-house, 4-staged artifact rejection pipeline applied to each electrode independently. This approach is adapted from Herman et al. (2019). First, the power spectrum for each electrode and each epoch was evaluated for 60 Hz noise utilizing Welch's power spectral density estimate method in MATLAB (www.mathworks.com). Any epoch that showed a frequency peak greater than 10 Hz with a topographical prominence greater than 200 μV/Hz was rejected. Next, the mean-square error (MSE) for each electrode and each epoch was calculated relative to zero to detect low amplitude signals suggesting electrodes that were disconnected, loose, or outside the brain. Any epoch with MSE less than 200 μV^2 was rejected. Third, a different MSE value for each electrode and each epoch was calculated as the difference between each individual epoch and the mean voltage timecourse for those epochs averaged within-subject. If an epoch deviated too far from the mean timecourse by having an MSE >3000 μV^2, then that epoch would be rejected. However, if too many epochs were rejected at this step, such as in the case of very noisy electrodes, then only the noisiest epochs up to 20% of the total epochs would be rejected. The rejection threshold of 20% was selected to balance considerations of noisy data and sample size as in prior work from our group (Herman et al., 2019). Finally, the standard deviation (SD) was calculated for each electrode across epochs. For event-level epochs, any epoch with one or more samples with a voltage greater than 5 SD was rejected. For block-level epochs, any epoch where more than 1% of samples (~655 samples) exceeded 5 SD was rejected. This pipeline rejected 16.50% of block epochs and 20.31% of event epochs.

2.5. Time-frequency analysis

Time-frequency analysis was implemented for all regions of interest (ROIs defined below) to compare sustained and transient changes across multiple frequency bands. Raw power for frequencies between 0 and 140 Hz was extracted from each electrode and epoch using the Morlet wavelet transform in MATLAB. Next, because the wavelet transform maintains the sampling rate of the original voltage data, down sampling was performed by averaging over 32 ms (event epochs) and 250 ms (block epochs) non-overlapping windows. The average down sampled power was calculated across all trials for each electrode within the ROIs and log-transformed. Finally, the log power was baselined by subtracting the average log power at each frequency 16s pre and post-task phases for block epochs and the 0.5s pre-stimulus for event epochs. Wavelet transform has greater frequency resolution at lower frequencies. To improve the visualization of power changes across a broad range of frequencies (0–140 Hz), spline interpolation across frequencies for each time point was applied prior to plotting the time-frequency results, so that samples in the frequency domain at each time point were evenly spaced at each integer between 0 and 140 Hz. Results of time-frequency analysis are shown in Supplementary Fig. S1.

2.6. Broadband gamma power extraction and Z-score transformation

We used the frequency range 40–115 Hz to investigate changes in broadband gamma power. Previous work has established that behavioral tasks evoke a characteristic increase in local cortical broadband gamma activity, along with increases in delta-theta (1–8 Hz) and decreases in alpha-beta (8–25 Hz) activity (Crone et al., 2006; Herman et al., 2019; Miller et al., 2014; Mukamel et al., 2005; Tallon-Baudry et al., 2005). This pattern was replicated in our analysis of visual cortical responses to transient events (Supplementary Fig. S1B). We focused our analyses on broadband gamma activity because prior work cited above shows that gamma activity has higher spatiotemporal resolution than signals in lower frequency ranges and is more closely associated with local population neuronal firing and BOLD fMRI signals. Our analysis of spectral changes across subjects confirmed robust changes from baseline within the 40–115 Hz range (Supplementary Fig. S1). Although changes in power were also observed in higher frequencies, we chose an upper cut-off of 115 Hz to avoid the artifact that may have been present in some of the data at 120 Hz, a harmonic of 60 Hz.

Broadband gamma (40–115 Hz) signal was extracted with a zero-phase, 40th order, Butterworth band-pass filter, created and applied in MATLAB across epochs. After filtering, 1s was removed from either side of the block and event-level epochs to eliminate filter edge effects. The final epoch size was 64s and 2s for block and events, respectively. Raw

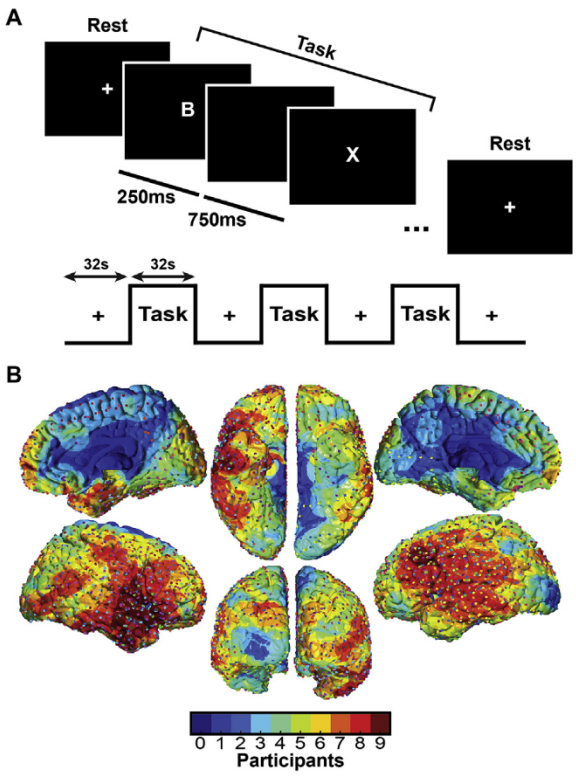

Fig. 1. Continuous performance task (CPT) and subdural electrode distribution. (**A**) CPT task design included two interleaved blocks, rest and task, each lasting for 32s. During the task phase, 32 English letters were presented for 250 ms at a rate of 1 Hz. Participants were instructed to respond with a right-handed button press for all 'X' letter presentations. (**B**) Participant (N = 11) cortical surface, intracranial electrodes on a common MNI-space brain surface. The electrode density map is shown for overlapping electrode territories defined as 15 mm radial distance from each electrode center, demonstrating the number of participants for which electrodes contribute at each point on the brain surface. The maximum electrode coverage was 9 participants in some brain regions. Each round color point on the brain surface map corresponds to an individual electrode and the point color is specific to an individual participant. A total of 1,908 electrodes were included in the analyses.

broadband gamma power was calculated by squaring the filtered gamma voltage. The raw gamma power was then binned in non-overlapping 256 sample (250 ms) and 32 sample (31.25 ms) time segments for block and event-level epochs, respectively. Next one final artifact rejection measure was employed. For event-level epochs, epochs were rejected if the binned gamma power at any time exceeded 20 SD of the mean for that electrode within each subject. For block-level epochs, samples with binned gamma power exceeding 7 SD of the mean for that electrode within each subject were replaced with "not a number" (NaN in MATLAB nomenclature) in order to preserve the epoch for analysis. The remaining epochs were averaged for each patient and z-score transformed using the mean and SD of the gamma power across block and event epoch specific baseline periods (block epoch baseline: 16s pre-block onset and 16s post-block offset; event epoch baseline: 500 ms prior to letter onset).

2.7. Mapping Z-scored gamma power to standard MNI brain surface and regions of interest (ROI)

Z-scored gamma power was mapped to the standard MNI vertices mesh brain surface utilizing the approach detailed by Herman et al. (2019). Briefly, we used each patient's post-op CT, post-op MRI and pre-op MRI to coregister their electrode locations into MNI space using BioImage Suite (http://bioimagesuite.yale.edu/). The MNI Colin 22 brain template was then used to generate a triangular mesh cortical surface representation in BioImage Suite and the 3-dimensional location of each electrode contact was assigned to the nearest vertex on the triangular mesh.

To map gamma power z-scores at each time point to the standard MNI brain surface, we first assigned z-score values in spherical regions surrounding each electrode within individual subjects, and then performed a weighted average of these values across subjects as described in Herman et al. (2019). Statistical analyses (see below) were performed across the data from individual subjects prior to taking the weighted average.

Anatomical ROIs were acquired from the SPM12 (www.fil.ion.ucl.ac.uk/spm) toolbox MarsBaR (voxel size = 2x2x2mm) (Tzourio-Mazoyer et al., 2002). Two main categories of ROIs were selected corresponding to both previous findings in the fMRI attention literature and the task demands of the CPT paradigm: DMN and visual processing regions. DMN ROIs included the PC (Precuneus in MarsBaR), VMP (Frontal_Sup_Medial, Frontal_Med_Orb, and Frontal_Sup_Orb in MarsBaR), PIPL (Angular in MarsBaR), and AMT (Hippocampus, ParaHippocampal, Temporal_Pole_Mid, and Temporal_Pole_Sup in MarsBaR) (Fig. 2A). The visual processing ROIs included V1 (Calcarine in MarsBaR) and FG (Fusiform in MarsBaR) (Fig. 2A). V1 and FG were included for their known roles in processing of visual stimuli and written letters (Cohen and Dehaene, 2004; Harris et al., 2016). In addition, because of individual differences in the spatial extent of nodes within the DMN as determined by functional imaging, functional DMN ROIs were also examined in comparison to the anatomical ROIs acquired from MarsBaR (Braga and Buckner, 2017; Shirer et al., 2012). Functional ROIs were acquired from a 90 ROI atlas (https://findlab.stanford.edu/functional_ROIs.html) (Shirer et al., 2012). The functional ROIs may better represent the underlying functional architecture than the anatomical ROIs, but yielded lower sample sizes with similar findings and therefore results from the functional ROIs are shown as Supplementary Figs. (S2 and S3). Total number of participants and electrodes within the anatomical and functional ROIs are reported in Supplementary Table S1.

We next mapped the functional and MarsBaR-derived anatomical ROIs in MNI space onto the vertices of the brain surface mesh, also in MNI space. This was performed by finding all vertices within a threshold distance of 1.5 mm from the center of each voxel in the corresponding ROIs. Any vertex found within the distance threshold of an ROI voxel was attributed to that ROI in the vertices brain surface mesh. Because voxels deeper in the brain were further away from the vertices of the brain surface mesh, exceeding the distance threshold, these voxels were automatically excluded from the vertex-space ROI. The projection procedure described above was satisfactory for all ROIs except FG, where there were notable regions on the vertices mesh surface (appearing as "holes") that were excluded from the FG ROI that should have been included. This outcome was due to a greater distance between the ROI voxels and vertices mesh along the ventral surface of the MNI brain, because the distance threshold used for the other ROIs was too shallow for this region. Therefore for the FG ROI, an initial voxel-to-vertex projection procedure was implemented where the FG ROI voxels were moved in the vertical direction to the nearest vertices on the ventral surface of the brain surface mesh. Because we found very similar results in the two hemispheres for these DMN and visual regions, to increase statistical power all ROI analyses combined results across the bilateral hemispheres for each ROI.

2.8. Model of expected BOLD fMRI timecourses and fMRI brain maps

To relate the gamma power EEG timecourses to BOLD signal dynamics, the gamma power z-score timecourse for the group weighted average at each brain mesh vertex was convolved with the canonical HRF commonly used in fMRI analysis. We used default HRF parameters in the SPM_HRF.m file (https://www.fil.ion.ucl.ac.uk/spm/) with a peak time of 5.1s and an undershoot trough time of 15.8s. The HRF was resampled to correspond with the electrophysiological time bins and convolved with the gamma power timecourses in MATLAB. To model the expected

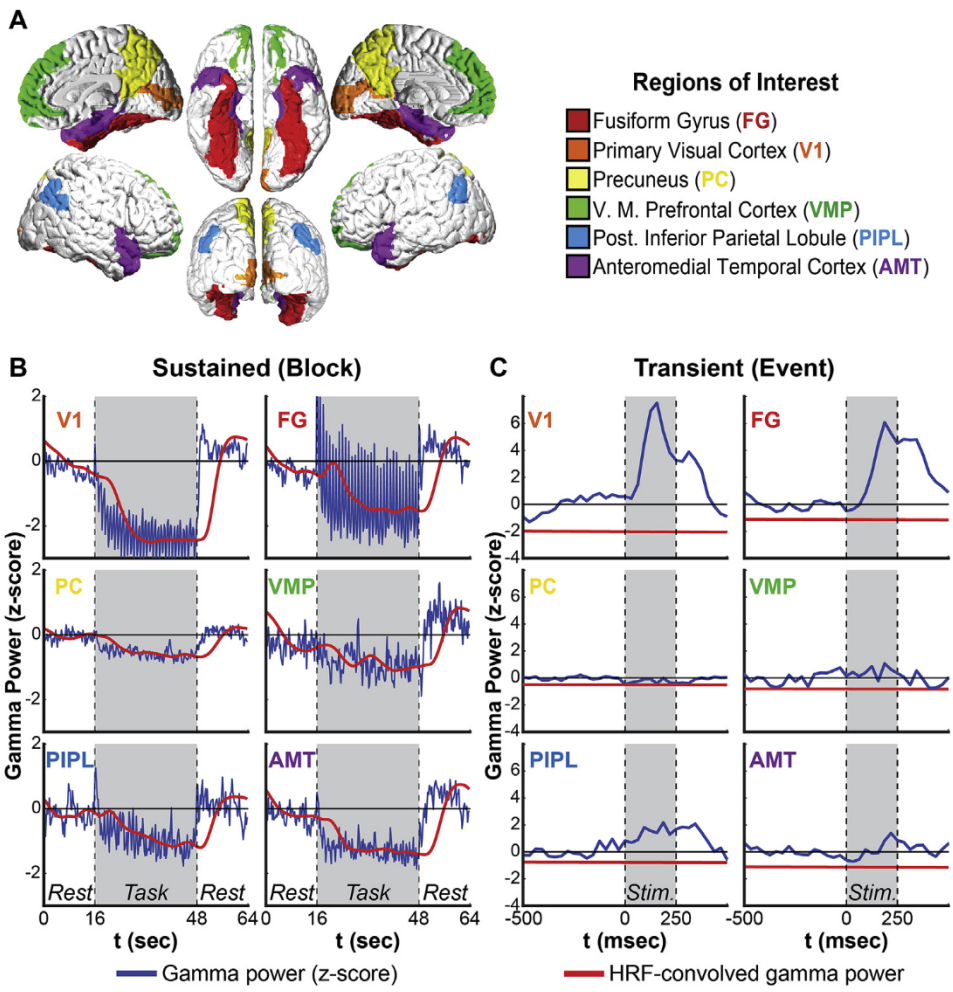

Fig. 2. Default mode and visual networks show sustained gamma power decreases in task blocks, but visual networks show transient signal increase with each stimulus
. **(A)** Selected anatomical regions of interest (ROIs) for analysis: fusiform gyrus (FG), primary visual cortex (V1), precuneus (PC), ventral medial prefrontal cortex (VMP), posterior inferior parietal lobule (PIPL), and anterior medial temporal cortex (AMT). **(B)** Block-level mean gamma power z-score timecourses across subjects (N = 11, see Supplementary Table S1 for sample size by region) for each ROI (blue traces) and mean HRF-convolved gamma power z-score timecourses (red traces). The epoch displayed includes 16s of the rest phase immediately preceding and following the task block. All ROIs exhibit sustained gamma power decreases during the task phase compared to rest. V1 and FG also show prominent transient rhythmic (1 Hz) increases throughout the task phase corresponding with the presentation of task letter stimuli (cf. part C). HRF-convolved gamma power captures the sustained decrease dynamic of each ROI but neglects the transient increases within V1 and FG. **(C)** Event-level mean gamma power z-scores (blue traces) across subjects (N = 11, see Supplementary Table S1 for sample size by region) and mean HRF-convolved gamma power z-scores (red traces) timecourses within each ROI. The epoch displayed includes 500 ms prior to letter onset and 500 ms following letter onset. V1 and FG show transient increases in gamma power for task event stimuli, absent in all other ROIs except for small increases in PIPL. HRF-convolved gamma power is insensitive to the event-level transient changes in V1 and FG.

block-level BOLD signal timecourses for each ROI, the HRF-convolved gamma power was averaged across all vertices attributed to each ROI (Fig. 2B; Supplementary Fig. S2B). To model the expected event-level BOLD signal timecourse dynamics for each ROI, we cut event epochs from the block HRF-convolved gamma power timecourses and then averaged across the event-level epochs (Fig. 2C; Supplementary Fig. S2C).

To map the expected block-level fMRI changes in a format similar to fMRI brain maps (Fig. 4) we calculated the difference between the mean HRF-convolved gamma power for task (32s) vs. baseline (16s pre- and post-task) phases for all vertices. This produced a single baseline minus task HRF-convolved gamma power value for each vertex. Positive and negative vertex values were mapped to the structural MRI MNI brain surface utilizing a 3-staged projection and visualization procedure. First, each voxel in the MNI brain was assigned the HRF-convolved gamma power signal value of its nearest vertex on the brain mesh in MNI space, with a maximum voxel center to vertex distance of 1 mm in the X, Y or Z direction so that only superficial voxels were considered. Next, to improve visualization on the MNI brain, all voxels within 8 mm in the X, Y or Z direction from the initial voxels were given the same values. If an individual voxel was found within 8 mm of multiple initial voxels, then the final value for this voxel was the average HRF-convolved gamma power value across those corresponding initial voxels. Finally, to eliminate voxels that were distributed outside the brain in the previous step, a whole-brain mask was applied to set the value of voxels outside the brain to zero. The final positive and negative HRF-convolved gamma power MNI brain images were converted to NIfTI format and visualized in MRIcron (https://www.nitrc.org/projects/mricron).

2.9. Statistical analysis of ROI gamma power

Statistical significance testing was assessed on the mean ROI z-scored gamma power timecourses across subjects. The maximum and minimum z-scored gamma power value was found during baseline and task phases of block (baseline = 16s pre-task; task = 32s-task block) and event-level epochs (baseline = 500 ms pre-stimulus; task = 250 ms post-stimulus) within all available ROIs for each participant (N = 11 participants). Two-tailed paired *t*-tests compared baseline versus task for block and event-level epochs across participants. The alpha significance level for these *t*-tests was Holm-Bonferroni corrected by the number ROIs tested within the visual network (V1 and FG) and DMN (PC, VMP, PIPL, and AMT) with threshold $P < 0.05$.

3. Results

The primary aim of this investigation was to assess the sustained and transient changes in DMN and visual cortical networks associated with dynamic attentional demands at both block and event-level temporal scopes. A secondary goal was to relate these EEG signals to modeled BOLD responses to allow for direct comparison to previous investigations of similar block design paradigms utilizing fMRI. The following summarizes the results that meet these two experimental goals.

3.1. Behavioral performance

The CPT paradigm was used in this study including both block (rest versus task phases) and event (letter presentation) epochs (Fig. 1A).

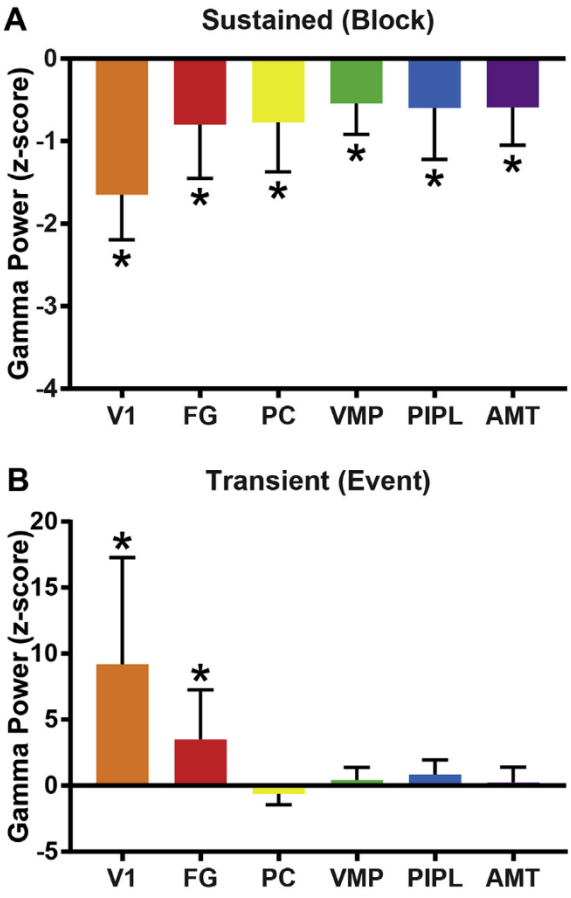

Fig. 3. Statistical analysis of sustained and transient gamma power signal dynamics.
(A) Sustained or block-level signal change analysis. Mean and standard deviation (SD) values for the difference between the minimum z-scored gamma power during rest (16s pre-task block) and task phases (32s). $^*P < 0.05$, Holm-Bonferroni-corrected two-tailed paired *t*-test. All ROIs exhibited a statistically significant decrease in gamma power during the task phase compared to rest. (**B**) Transient or event-level signal change analysis. Mean and SD values for the difference between the maximum z-scored gamma power pre-letter (500 ms) and post-letter (250 ms) presentation phases. $^*P < 0.05$, Holm-Bonferroni-corrected two-tailed paired *t*-test. V1 and FG were statistically significant for gamma power increases after letter presentation compared to baseline. All other ROIs were not statistically significant. N = 11 subjects, same data as in Fig. 2.

Participants completed a total of 71 runs, or 710 blocks (mean = 6.45 runs or ~65 blocks per subject over multiple testing sessions), with a block defined as a single rest and task phase cycle. Due to interruptions during the testing session, 3 additional runs totaling 18 blocks were incomplete but were included for further analysis. 81 blocks were removed due to noisy TTL pulse signal that prevented event-time detection. Of the remaining 647 CPT blocks, there were a total of 19,406 letter event stimuli (target letters = 4,632; non-target letters = 14,774). Participants correctly responded to 95.25% of all target letter presentations and incorrectly responded to 0.97% of all non-target letters, suggesting participants understood the task instructions and were largely attentive during the task phase.

3.2. Sustained and transient gamma power signal changes

Diverging block and event-level signal dynamics were observed across ROIs. Block-level z-scored gamma power timecourses revealed a sustained decrease during the task phase across all DMN and visual ROIs, compared to the rest phase (Fig. 2B; blue traces). Sustained decreases were tested for statistical significance by comparing baseline (16s pre-task phase onset) and task phase nadir or minimum values using a two-tailed paired *t*-test across subjects. The mean block minimum z-scored gamma power value difference between baseline and task was computed and showed consistent decreases for each ROI during the task phase (Fig. 3A). Task phase minimum gamma power values were statistically significant compared to baseline for all regions (Holm-Bonferroni-corrected $P < 0.05$). Similar sustained decreases in gamma power were observed among the functional DMN ROIs (Supplementary Fig. S2B), although minimum gamma power values were statistically significant compared to baseline for only VMP, likely due to reduced statistical power among the functional DMN ROIs because less electrodes were included within each ROI (Supplementary Table S1; Supplementary Fig. S3A). In addition to group analyses, individual electrode responses during the task phase also showed sustained decreases in gamma power for all ROIs (Supplementary Fig. S6A).

Although both the visual and DMN regions showed sustained, gamma power decreases during task blocks, event-related analyses revealed transient gamma power increases in V1 and FG corresponding with each of the letter presentations (Fig. 2C; blue traces). These transient changes examined directly with event-level epochs showed prominent gamma power increases in V1 and FG following the letter presentations, returning to baseline after approximately 500 ms. Meanwhile, PC, VMP, and AMT showed no and PIPL marginal increases immediately following the onset of letter stimuli. The peak or maximum value for each ROI was found within 500 ms pre-letter onset (baseline) and 250 ms post-letter onset (event) across subjects and tested for statistical significance using a two-tailed paired *t*-test. The mean event maximum z-scored gamma power value difference between baseline and event was computed for each ROI (Fig. 3B). Statistically significant event-related z-score gamma power increases between baseline and event phases were found for V1 and FG ($P < 0.05$, Holm-Bonferroni-corrected). Functional DMN ROIs demonstrated no statistically significant changes in gamma power for individual task events, corresponding with findings from anatomical ROIs (Supplementary Figs. S2C and S3B). Again, individual electrode transient responses to letters mirror group findings, including event-related increases in gamma power for V1 and FG but minimal changes in the other ROIs (Supplementary Fig. S6B). Moreover, event-related transient changes in gamma power were similar for both target (letter X) and non-target stimuli suggesting the mean gamma power responses across all stimuli within the selected ROIs were not disproportionally driven by a stimulus subtype (Supplementary Figs. S4 and S5).

3.3. EEG and BOLD signal dynamic comparison

Due to the unique signal sources and diverging temporal resolution of EEG and fMRI, it is challenging to directly compare results captured with these two important methods. Block design paradigms such as the CPT task are commonly used in fMRI (e.g., Killory et al., 2011). To better relate the current EEG results with those of previous fMRI investigations, a canonical HRF-convolution was applied to the z-scored gamma power signal to model a corresponding BOLD response (see Materials and Methods section). The HRF-convolved signal revealed sustained decreases across all ROIs and introduced some temporal delay and smoothing as expected for fMRI signals (Fig. 2B; red traces; see also Supplementary Fig. S2B red traces). These results largely correspond with the z-scored gamma power signal traces by showing overall sustained decreases in all regions. Meanwhile, the HRF-convolved gamma power is insensitive to the transient changes in gamma power for event epochs that occur at a rate of 1 Hz during the task phase in V1 and FG (Fig. 2C; red traces; see also Supplementary Fig. S2C red traces). This is consistent with the poor temporal resolution of the BOLD response for which temporal jitter is necessary to resolve closely spaced events (Huettel et al., 2014); and the lack of jitter in the present 1 Hz visual stimuli. Therefore, there is a larger disparity between the HRF-convolved signal and gamma power timecourses for transient events, whereas the sustained signals are more similar for these two modalities.

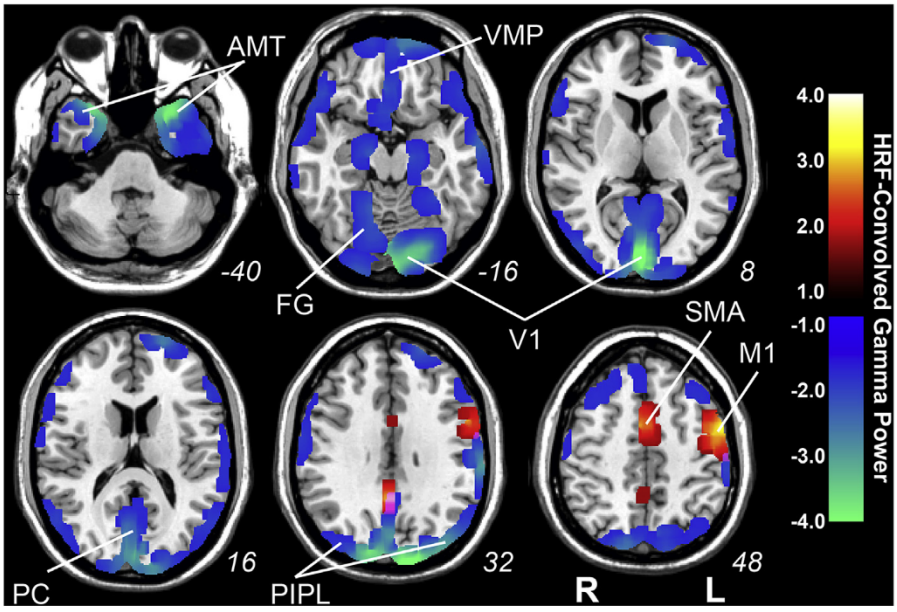

Fig. 4. MRI voxel brain map of sustained HRF-Convolved gamma power. Displayed are mean HRF-convolved gamma power z-score difference values between baseline and task phases for each vertex projected to voxel MNI space. The warm and cool colors represent positive and negative HRF-convolved gamma power compared to baseline, respectively. Signal decreases are present among default mode network regions, including PC (precuneus), VMP (ventral medial prefrontal cortex), PIPL (posterior inferior parietal lobule), and AMT (anterior medial temporal cortex), and visual network regions, including V1 (primary visual cortex) and FG (fusiform gyrus). Signal increases are found in SMA (supplementary motor area) and left M1 (primary motor cortex), corresponding to the button response demands of the paradigm. N = 11 subjects, same data as in Figs. 2 and 3.

To further relate the current results to previous fMRI studies, HRF-convolved gamma power signal in vertices space was applied to the MNI brain in voxel space to obtain maps in similar format to those typically used for fMRI results. This visualization recapitulates sustained findings from the z-scored gamma power and HRF-convolved gamma power timecourses (Fig. 2B), including decreases in the DMN (e.g., PC, VMP, PIPL, AMT), and decreases in visual processing regions, like V1 and FG (Fig. 4). These intracranial EEG-based results match previously published BOLD fMRI studies with the same CPT task in normal subjects, showing fMRI decreases in visual cortex and posterior cingulate/precuneus DMN regions (Killory et al., 2011). There are also regional increases found in the supplementary motor area (SMA) and left hemisphere primary motor cortex (M1) corresponding with the right-handed button presses required by participants in order to respond to target letters (Fig. 4), again in agreement with prior fMRI work with the same CPT task (Killory et al., 2011).

4. Discussion

The current study reveals both sustained and transient electrophysiological changes associated with dynamic attention-based task demands and visual stimulus presentation. Recapitulating previous findings in the fMRI literature, the DMN, including the PC, VMP, and AMT are suppressed for the duration of active task phases compared to rest phases. This result supports the well-described role of the DMN as a task-negative network and therefore enhanced during rest and depressed during task engagement (Fox et al., 2005; Gusnard et al., 2001; Shulman et al., 1997). Prior work suggests that sustained depressed electrophysiological activity may occur in DMN during tasks (e.g., Ossandon et al., 2011), and the present results confirm that sustained DMN decreases occur in a classic mixed block and event design commonly used in fMRI studies. These block onset-offset changes suggest an attentional switching mechanism to optimize brain state to maximize performance, as has been supported by previous studies (Monsell, 2003; Weissman et al., 2006; Herman et al., 2019). A potential driver of these attentional state changes are arousal and salience networks, that include anterior insula, cingulate cortex, thalamus, and brainstem (Saper et al., 2005; Seeley et al., 2007).

V1 and FG also showed notable sustained gamma power decreases during the task phase. Although sustained fMRI decreases in visual cortex have been reported previously in fMRI studies during task blocks (Killory et al., 2011; Olsen et al., 2013; Shmuel et al., 2006; Singh and Fawcett, 2008; Smith et al., 2000, 2004) this signal dynamic is surprising in the context of a visual-based paradigm where we would expect the visual processing network to respond with increased activity during the task phase corresponding with visual stimuli presentation. The current investigation offers an explanation revealing that the prolonged average gamma power response of V1 and FG is to decrease, yet a transient increase is also registered for each task stimulus. Therefore, a block versus an event-level analysis of these regions would generate competing results for the direction of signal change in V1 and FG. As modeled by the HRF-convolved gamma power in the current study, the BOLD response would be sensitive to the sustained decrease in V1 and FG during the task block but may neglect the transient changes at the event-level due to the delayed HRF response when stimuli are presented at regular closely spaced intervals (without temporal jitter). This also helps resolve the paradox of several fMRI studies which show visual cortex and visual association cortex increases with event-related design when temporal jitter is present, but fMRI decreases during block-design-based analyses (Harris et al., 2016; Killory et al., 2011; Liu et al., 2011; Olsen et al., 2013; Singh and Fawcett, 2008; Smith et al., 2000). Indeed, a previous study from our group recorded BOLD signal responses while participants engaged in the same CPT paradigm used here, demonstrating fMRI decreases in visual cortex and posterior cingulate/precuneus DMN regions corresponding with the block-level, HRF-convolved gamma power changes observed with intracranial EEG in the present study (Killory et al., 2011).

The neuronal and behavioral explanation for the sustained decrease in V1 and FG is unresolved. Some have hypothesized that decreased cortical gamma activity may suppress signaling not relevant to task demands (Lachaux et al., 2008; Herman et al., 2019). Perhaps, this decrease represents a refractory period in visual networks following the transient increase from repeated stimuli presentation. Alternatively, the visual networks decrease may represent a state change that serves to improve performance in a repetitive stimulus presentation paradigm by, for example, enhancing signal-to-noise through attention-related suppression of background neural activity (Smith et al., 2000, 2004). In addition, the concordance of sustained activity decreases in DMN and in visual networks during task blocks raises the intriguing possibility that these activity decreases may be linked. Previous work proposes that activity in task-positive regions (e.g., dorsal attention network) may drive suppression in the DMN, suggested by the latency in signal between task positive and negative networks observed with intracranial EEG, and a

similar mechanism may underly the changes currently observed in visual networks (Raccah et al., 2018). Further work is needed to distinguish these possibilities and to investigate underlying mechanisms.

A persistent challenge in neuroscience is interpreting results between methodologies with unique sources, for example, between fMRI and EEG. In the current investigation, it was a priority to relate the intracranial EEG findings with a modeled BOLD response due to the prominence of fMRI in the attention block design literature. Accordingly, the current results support that the origin of the BOLD signal decreases during task engagement is reduced population neuronal firing as measured by broadband gamma power, corresponding with previous findings (Shmuel et al., 2006). This excludes vascular sources for the BOLD signal decrease in attention-manipulating block design paradigms.

The results from this study are limited by the use of participants with epilepsy. While we aimed to limit this confound by eliminating data with subclinical or clinical epileptic activity, the attention networks investigated may be permanently altered by epilepsy and its comorbidities, limiting generalization to the healthy nervous system. However, the correspondence between the current results and previous investigations with healthy controls tempers this concern. Another challenge is that the electrode coverage was sparse in certain regions and absent in subcortical regions. Future investigations may consider utilizing high density scalp EEG or MEG and source localization or a larger intracranial EEG dataset to tackle these primary limitations of the current investigation. Finally, the current investigation has focused on DMN suppression with engagement in a CPT task, but there is also strong evidence for DMN activation with internally-directed task, for example, thinking of the past or future (Dastjerdi et al., 2011; Fox et al., 2018). Examining the drivers of signal increases and decreases in DMN will be critical to better understanding the relationship between the DMN and competing cortical networks.

5. Conclusions

Attention engagement and disengagement is a constant behavior in daily life. Previous fMRI investigations have shown sustained increases in task positive networks and decreases in task negative networks when performing an active, externally-focused task. There are also transient dynamics that are driven by the presentation of stimuli. The current investigation confirms these results with direct electrophysiological recordings by showing there are both sustained decreases in the DMN and visual networks, as well as transient increases in visual networks while performing a visual attention task. Unique to this study, is the direct comparison between block and event-level attention states revealing a sustained decrease and transient increase in V1 and FG. This result is challenging to assess in fMRI where the signal temporal dynamics biases observation of prolonged effects. These results support dynamic state changes in the DMN and sensory cortices with updating task demands. While not directly tested in the current investigation, these network state mechanisms may play a role in normal task performance and help explain instances of cognitive impairment.

Funding

This work was supported by the Betsy and Jonathan Blattmachr Family, the Loughridge Williams Foundation and by NIH R01 NS055829 (H.B.), the Natural Science Foundation of China 11772242, a China Scholarship Council Fellowship (J.L.) and NINDS T32 NS007224 (S.K.).

Declarations of interest

None.

Acknowledgments

We are grateful to the Yale New Haven Hospital Epilepsy Clinical Team, and to the patients who volunteered their time to participate in these studies.

Appendix A. Supplementary data

Supplementary data to this article can be found online at https://doi.org/10.1016/j.neuroimage.2019.07.016.

References

Bai, X., Vestal, M., Berman, R., Negishi, M., Spann, M., Vega, C., Desalvo, M., Novotny, E.J., Constable, R.T., Blumenfeld, H., 2010. Dynamic time course of typical childhood absence seizures: EEG, behavior, and functional magnetic resonance imaging. J. Neurosci. 30, 5884–5893.

Beck, L.H., Bransome Jr., E.D., Mirsky, A.F., Rosvold, H.E., Sarason, I., 1956. A continuous performance test of brain damage. J. Consult. Psychol. 20, 343–350.

Berman, R., Negishi, M., Vestal, M., Spann, M., Chung, M.H., Bai, X., Purcaro, M., Motelow, J.E., Danielson, N., Dix-Cooper, L., Enev, M., Novotny, E.J., Constable, R.T., Blumenfeld, H., 2010. Simultaneous EEG, fMRI, and behavior in typical childhood absence seizures. Epilepsia 51, 2011–2022.

Braga, R.M., Buckner, R.L., 2017. Parallel interdigitated distributed networks within the individual estimated by intrinsic functional connectivity. Neuron 95, 457–471.

Bressler, D., Spotswood, N., Whitney, D., 2007. Negative BOLD fMRI response in the visual cortex carries precise stimulus-specific information. PLoS One 2.

Cohen, L., Dehaene, S., 2004. Specialization within the ventral stream: the case for the visual word form area. Neuroimage 22, 466–476.

Corbetta, M., Shulman, G.L., 2002. Control of goal-directed and stimulus-driven attention in the brain. Nat. Rev. Neurosci. 3, 201–215.

Crone, N.E., Sinai, A., Korzeniewska, A., 2006. High-frequency gamma oscillations and human brain mapping with electrocorticography. Prog. Brain Res. 159, 275–295.

Dastjerdi, M., Foster, B.L., Nasrullah, S., Rauschecker, A.M., Dougherty, R.F., Townsend, J.D., Chang, C.T., Greicius, M.D., Menon, V., Kennedy, D.P., Parvizi, J., 2011. Differential electrophysiological response during rest, self-referential, and non-self-referential tasks in human posteromedial cortex. Proc. Natl. Acad. Sci. U.S.A. 108, 3023–3028.

Dosenbach, N.U.F., Visscher, K.M., Palmer, E.D., Miezin, F.M., Wenger, K.K., Kang, H.S.C., Burgund, E.D., Grimes, A.L., Schlaggar, B.L., Petersen, S.E., 2006. A core system for the implementation of task sets. Neuron 50, 799–812.

Foster, B.L., Dastjerdi, M., Parvizi, J., 2012. Neural populations in human posteromedial cortex display opposing responses during memory and numerical processing. Proc. Natl. Acad. Sci. U.S.A. 109, 15514–15519.

Fox, K.C.R., Foster, B.L., Kucyi, A., Daitch, A.L., Parvizi, J., 2018. Intracranial electrophysiology of the human default network. Trends Cognit. Sci. 22, 307–324.

Fox, M.D., Snyder, A.Z., Vincent, J.L., Corbetta, M., Van Essen, D.C., Raichle, M.E., 2005. The human brain is intrinsically organized into dynamic, anticorrelated functional networks. Proc. Natl. Acad. Sci. U.S.A. 102, 9673–9678.

Gonzalez-Castillo, J., Saad, Z.S., Handwerker, D.A., Inati, S.J., Brenowitz, N., Bandettini, P.A., 2012. Whole-brain, time-locked activation with simple tasks revealed using massive averaging and model-free analysis. Proc. Natl. Acad. Sci. U.S.A. 109, 5487–5492.

Gusnard, D.A., Raichle, M.E., Raichle, M.E., 2001. Searching for a baseline: functional imaging and the resting human brain. Nat. Rev. Neurosci. 2, 685–694.

Harris, R.J., Rice, G.E., Young, A.W., Andrews, T.J., 2016. Distinct but overlapping patterns of response to words and faces in the fusiform gyrus. Cerebr. Cortex 26, 3161–3168.

Herman, W.X., Smith, R.E., Kronemer, S.I., Watsky, R.E., Chen, W.C., Gober, L.M., Touloumes, G.J., Khosla, M., Raja, A., Horien, C.L., Morse, E.C., Botta, K.L., Hirsch, L.J., Alkawadri, R., Gerrard, J.L., Spencer, D.D., Blumenfeld, H., 2019. A switch and wave of neuronal activity in the cerebral cortex during the first second of conscious perception. Cerebr. Cortex 29, 461–474.

Huettel, S.A., Song, A.W., McCarthy, G., 2014. In: Functional Magnetic Resonance Imaging, third ed. Sinauer Associates, Inc., Sunderland, MA.

Jerbi, K., Vidal, J.R., Ossandon, T., Dalal, S.S., Jung, J., Hoffmann, D., Minotti, L., Bertrand, O., Kahane, P., Lachaux, J.P., 2010. Exploring the electrophysiological correlates of the default-mode network with intracerebral EEG. Front. Syst. Neurosci. 4, 27.

Killory, B.D., Bai, X., Negishi, M., Vega, C., Spann, M.N., Vestal, M., Guo, J., Berman, R., Danielson, N., Trejo, J., Shisler, D., Novotny Jr., E.J., Constable, R.T., Blumenfeld, H., 2011. Impaired attention and network connectivity in childhood absence epilepsy. Neuroimage 56, 2209–2217.

Lachaux, J.P., George, N., Tallon-Baudry, C., Martinerie, J., Hugueville, L., Minotti, L., Kahane, P., Renault, B., 2005. The many faces of the gamma band response to complex visual stimuli. Neuroimage 25, 491–501.

Lachaux, J.P., Jung, J., Mainy, N., Dreher, J.C., Bertrand, O., Baciu, M., Minotti, L., Hoffmann, D., Kahane, P., 2008. Silence is golden: transient neural deactivation in the prefrontal cortex during attentive reading. Cerebr. Cortex 18, 443–450.

Liu, Y., Shen, H., Zhou, Z., Hu, D., 2011. Sustained negative BOLD response in human fMRI finger tapping task. PLoS One 6, e23839.

Miller, K.J., 2010. Broadband spectral change: evidence for a macroscale correlate of population firing rate? J. Neurosci. 30, 6477–6479.

Miller, K.J., Honey, C.J., Hermes, D., Rao, R.P., Dennijs, M., Ojemann, J.G., 2014. Broadband changes in the cortical surface potential track activation of functionally diverse neuronal populations. Neuroimage 85 (2), 711–720.

Miller, K.J., Weaver, K.E., Ojemann, J.G., 2009. Direct electrophysiological measurement of human default network areas. Proc. Natl. Acad. Sci. U. S. A. 106, 12174–12177.
Mirsky, A.F., Rosvold, H.E., 1963. Behavioral and physiological studies in impaired attention. In: Votava, Z.e.a. (Ed.), Psychopharmacological Methods: Proceedings of a Symposium on the Effects of Psychotropic Drugs on Higher Nervous Activity. Pergamon Press, Oxford, pp. 302–315.
Mishra, A.M., Ellens, D.J., Schridde, U., Motelow, J.E., Purcaro, M.J., DeSalvo, M.N., Enev, M., Sanganahalli, B.G., Hyder, F., Blumenfeld, H., 2011. Where fMRI and electrophysiology agree to disagree: corticothalamic and striatal activity patterns in the WAG/Rij rat. J. Neurosci. 31, 15053–15064.
Monsell, S., 2003. Task switching. Trends Cognit. Sci. 7, 134–140.
Mukamel, R., Gelbard, H., Arieli, A., Hasson, U., Fried, I., Malach, R., 2005. Coupling between neuronal firing, field potentials, and fMRI in human auditory cortex. Science 309, 951–954. %U. http://www.sciencemag.org/content/309/5736/5951.abstract.
Mullinger, K.J., Mayhew, S.D., Bagshaw, A.P., Bowtell, R., Francis, S.T., 2014. Evidence that the negative BOLD response is neuronal in origin: a simultaneous EEG-BOLD-CBF study in humans. Neuroimage 94, 263–274.
Olsen, A., Ferenc Brunner, J., Evensen, K.A., Garzon, B., Landro, N.I., Haberg, A.K., 2013. The functional topography and temporal dynamics of overlapping and distinct brain activations for adaptive task control and stable task-set maintenance during performance of an fMRI-adapted clinical continuous performance test. J. Cogn. Neurosci. 25, 903–919.
Ossandon, T., Jerbi, K., Vidal, J.R., Bayle, D.J., Henaff, M.A., Jung, J.L., Minotti, L., Bertrand, O., Kahane, P., Lachaux, J.P., 2011. Transient suppression of broadband gamma power in the default-mode network is correlated with task complexity and subject performance. J. Neurosci. 31, 14521–14530.
Raccah, O., Daitch, A.L., Kucyi, A., Parvizi, J., 2018. Direct cortical recordings suggest temporal order of task-evoked responses in human dorsal attention and default networks. J. Neurosci. 38, 10305–10313.
Raichle, M.E., Snyder, A.Z., 2007. A default mode of brain function: a brief history of an evolving idea. Neuroimage 37, 1083–1090.
Ramot, M., Fisch, L., Harel, M., Kipervasser, S., Andelman, F., Neufeld, M.Y., Kramer, U., Fried, I., Malach, R., 2012. A widely distributed spectral signature of task-negative electrocorticography responses revealed during a visuomotor task in the human cortex. J. Neurosci. 32, 10458–10469.
Riccio, C.A., Reynolds, C.R., Lowe, P., Moore, J.J., 2002. The continuous performance test: a window on the neural substrates for attention? Arch. Clin. Neuropsychol. 17, 235–272.
Rushworth, M.F.S., Hadland, K.A., Paus, T., Sipila, P.K., 2002. Role of the human medial frontal cortex in task switching: a combined fMRI and TMS study. J. Neurophysiol. 87, 2577–2592.
Saper, C.B., Scammell, T.E., Lu, J., 2005. Hypothalamic regulation of sleep and circadian rhythms. Nature 437, 1257–1263.
Schridde, U., Khubchandani, M., Motelow, J.E., Sanganahalli, B.G., Hyder, F., Blumenfeld, H., 2008. Negative BOLD with large increases in neuronal activity. Cerebr. Cortex 18, 1814–1827.
Seeley, W.W., Menon, V., Schatzberg, A.F., Keller, J., Glover, G.H., Kenna, H., Reiss, A.L., Greicius, M.D., 2007. Dissociable intrinsic connectivity networks for salience processing and executive control. J. Neurosci. 27, 2349–2356.
Shirer, W.R., Ryali, S., Rykhlevskaia, E., Menon, V., Greicius, M.D., 2012. Decoding subject-driven cognitive states with whole-brain connectivity patterns. Cerebr. Cortex 22, 158–165.
Shmuel, A., Augath, M., Oeltermann, A., Logothetis, N.K., 2006. Negative functional MRI response correlates with decreases in neuronal activity in monkey visual area V1. Nat. Neurosci. 9, 569–577.
Shulman, G.L., Fiez, J.A., Corbetta, M., Buckner, R.L., Miezin, F.M., Raichle, M.E., Petersen, S.E., 1997. Common blood flow changes across visual tasks: II. Decreases in cerebral cortex. J. Cogn. Neurosci. 9 (5), 648–663.
Singh, K., Fawcett, I., 2008. Transient and linearly graded deactivation of the human default-mode network by a visual detection task. Neuroimage 41, 100–112.
Smith, A.T., Singh, K.D., Greenlee, M.W., 2000. Attentional suppression of activity in the human visual cortex. Neuroreport 11, 271–277.
Smith, A.T., Williams, A.L., Singh, K.D., 2004. Negative BOLD in the visual cortex: evidence against blood stealing. Hum. Brain Mapp. 21, 213–220.
Sohn, M.H., Ursu, S., Anderson, J.R., Stenger, V.A., Carter, C.S., 2000. The role of prefrontal cortex and posterior parietal carter in task switching. Proc. Natl. Acad. Sci. U.S.A. 97, 13448–13453.
Tallon-Baudry, C., Bertrand, O., Henaff, M.A., Isnard, J., Fischer, C., 2005. Attention modulates gamma-band oscillations differently in the human lateral occipital cortex and fusiform gyrus. Cerebr. Cortex 15, 654–662.
Tzourio-Mazoyer, N., Landeau, B., Papathanassiou, D., Crivello, F., Etard, O., Delcroix, N., Mazoyer, B., Joliot, M., 2002. Automated anatomical labeling of activations in SPM using a macroscopic anatomical parcellation of the MNI MRI single-subject brain. Neuroimage 15, 273–289.
Weissman, D., Roberts, K., Visscher, K., Woldorff, M., 2006. The neural bases of momentary lapses in attention. Nat. Neurosci. 9, 971–978.